



HAL
open science

Invertible Micelles Based on Ion-Specific Interactions of Sr $2+$ and Ba $2+$ with Double Anionic Block Copolyelectrolytes

Nico Carl, Sylvain Prevost, Ralf Schweins, Judith Houston, Isabelle Morfin,
Klaus Huber

► **To cite this version:**

Nico Carl, Sylvain Prevost, Ralf Schweins, Judith Houston, Isabelle Morfin, et al.. Invertible Micelles Based on Ion-Specific Interactions of Sr $2+$ and Ba $2+$ with Double Anionic Block Copolyelectrolytes. *Macromolecules*, 2019, 52 (22), pp.8759-8770. 10.1021/acs.macromol.9b01924 . hal-02396455

HAL Id: hal-02396455

<https://hal.science/hal-02396455>

Submitted on 5 Jan 2021

HAL is a multi-disciplinary open access archive for the deposit and dissemination of scientific research documents, whether they are published or not. The documents may come from teaching and research institutions in France or abroad, or from public or private research centers.

L'archive ouverte pluridisciplinaire **HAL**, est destinée au dépôt et à la diffusion de documents scientifiques de niveau recherche, publiés ou non, émanant des établissements d'enseignement et de recherche français ou étrangers, des laboratoires publics ou privés.

Invertible Micelles Based on Ion Specific Interactions of Sr^{2+} and Ba^{2+} with Double Anionic Block Copolyelectrolytes

Nico Carl,^{†,‡} Sylvain Prévost,[†] Ralf Schweins,[†] Judith E. Houston,[¶] Isabelle Morfin,[§] and Klaus Huber^{*,‡}

[†]*Large Scale Structures Group, DS, Institut Laue-Langevin, 71 Avenue des Martyrs, CS 20 156, 38042 Grenoble, France*

[‡]*Chemistry Department, University of Paderborn, Warburger Str. 100, 33098 Paderborn, Germany*

[¶]*Jülich Centre for Neutron Science, Forschungszentrum Jülich GmbH, Garching 85747, Germany*

[§]*Université Grenoble Alpes, LiPhy, 38000 Grenoble, France*

E-mail: klaus.huber@upb.de

Abstract

Polyelectrolytes show diverse ion-specific effects with a wide variety of ions. In the present work, we study the solution behavior of diblock copolymers with poly acrylate (PA) and poly styrenesulfonate (PSS) blocks in the presence of the earth alkaline cations Ca^{2+} , Sr^{2+} and Ba^{2+} . Micellization can be triggered by a variation of temperature. For Ca^{2+} this micelle formation occurs at high temperatures, while for Sr^{2+} and Ba^{2+} it occurs at high and low temperatures with an intermediate temperature regime of single chains. Small-angle neutron scattering on a partly deuterated block

copolymer unambiguously revealed that at low temperatures PSS/M²⁺ forms the core of the micelles, whereas at high temperatures PA/M²⁺ forms the core, effectively allowing to reverse the micelle structure by changing the temperature. This inversion of the micellar morphology, induced by a dual responsive behavior can be understood by using isothermal titration calorimetry and elucidating the thermodynamics of cation binding.

Introduction

Amphiphilic block copolymers self-assemble into structures ranging from spherical¹ to worm-like micelles² or vesicles.³ Extensive research has been conducted to develop block copolymers where one of the blocks responds to external stimuli such as temperature,⁴ pH,⁵ pressure⁶ or light⁷ in order to affect the hydrophobicity of the respective block and hence to switch between the monomeric and self-assembled state. So far, such stimuli or combinations thereof have been used to generate switchable emulsifiers,⁸ to control rheology⁹ or to release active agents.¹⁰ In order to create even more versatile systems research efforts were aiming at block copolymers where each of the two blocks responds to a different stimulus. Such systems were expected to accomplish an inversion of the micellar structure by reversibly addressing the stimulus of the two blocks one by one. Accordingly, the term schizophrenic micelles has been coined for these systems.^{11,12,12-19}

The underlying concept of many of such systems makes use of one block with an upper critical solution temperature (UCST) and a second block with a lower critical solution temperature (LCST). Furthermore, it is ensured that a significant temperature gap exists between the UCST and LCST.¹¹ Only such a gap makes accessible the state of single block copolymer chains in between the state of micelles and of inverted micelles.¹¹ However, a problem observed during those efforts was that in the regime where both blocks should be soluble the chains tend to aggregate.^{11,17,18} In the light of potential applications such as controlled uptake, transport or release of low molecular weight compounds these effects are undesirable

as they might provide cavities which keep back the cargo and prevent the complete release of it.

In the present work, we pursue a slightly different strategy to realize such an invertible system. Block copolymers of two negatively charged polyelectrolytes, sodium polyacrylate (PA) and sodium polystyrene sulphonate (PSS), are synthesized.^{20,21} Polyelectrolytes are commonly used as building blocks for block copolymers due to their water solubility, pH responsivity and the ability to form charge-stabilized self-assembled structures.^{1,22,23} The selection of PA and PSS is based on previous works,^{24,25} which demonstrated unambiguously, that the two polyanions interact specifically and in a different manner with alkaline earth cations. This interaction is temperature dependent whereby the temperature dependence also differs when going from PA to PSS.^{24,26}

In more detail, earth alkaline metal cations M^{2+} complex the anionic moieties of PA and neutralize the negative charges. This results in phase separation of the polymer at a critical concentration of $[M^{2+}]_c$, which depends on the PA concentration $[PA]$ ^{25,27}

$$[M^{2+}]_c = r_0 + m[PA] \tag{1}$$

with $[PA]$ being the concentration of PA monomer units, r_0 being the minimum concentration of M^{2+} required for precipitation and m being the stoichiometry of binding. Strikingly, the binding of M^{2+} to PA is endothermic with all three cations^{26,28,29} and phase separation is thus promoted by an increase of temperature²⁶, discernible in a decrease in r_0 with an increase of temperature.

In contrast, PSS shows a completely different phase behavior with earth alkaline cations. No macroscopic phase separation is observed in the presence of Ca^{2+} and Sr^{2+} .^{24,29} For Ba^{2+} a horizontal phase boundary according to

$$[Ba^{2+}]_c = r_0 \tag{2}$$

is observed.^{24,30,31} Above all, the binding of Ba^{2+} to the anionic moieties of PSS is dominated by an exothermic complexation²⁹ and r_0 decreases in this case with decreasing temperature.²⁴

We deliberately used the term phase separation instead of precipitation for all these cases as we are most likely dealing with a liquid-liquid phase separation (LLPS) of the dissolved polyelectrolytes neutralized via specific interactions with alkaline earth cations.³² In fact Muthukumar *et al.*³³ could demonstrate that the LLPS observed with Ba^{2+} and PSS obeys an UCST behavior. As the impact of temperature on the binding of Ba^{2+} to PA is inverse to the binding of Ba^{2+} to PSS, we have good reason to assume that the interaction with Ba^{2+} exhibits a LCST. Given that the interaction of PA with M^{2+} obeys a LCST behavior whereas the interaction of PSS with Ba^{2+} is of an UCST type, a combination of these two features in a block copolyelectrolyte may pave the road to invertible micelles with Ba^{2+} and PA-*b*-PSS diblock copolymers, in analogy to the concept pursued by Papadakis *et al.*^{11,17,18} It is this idea, which is at the center of the present work. A first step along this line has already been accomplished in a preceding work, in which we showed that these differing modes of interaction with Ca^{2+} can be used to self-assemble PA-*b*-PSS block copolymers into well-defined micelles.²⁰

Herein, we report on the effect of temperature on the self-assembly of PA-*b*-PSS in the presence of Ca^{2+} , Sr^{2+} and Ba^{2+} . Small-angle neutron scattering in combination with isothermal titration calorimetry is employed to unambiguously prove that it is possible to create a invertible system with this type of block copolymer and that the inversion of the micelle structure passes a regime of single chains. At the same time, the present results introduce multivalent cations in combination with block copolyelectrolytes as a new toolbox for temperature responsive polymers and dual responsive systems.

Experiments and Data Analysis

Materials. Light water was purified using a Milli-Q-system, heavy water (D_2O , Euriso-top, France, 99.90 atom% deuterium) was filtered with 100 nm PVDF filter (Merck Millex MPSLVV033RS) prior to use. $CaCl_2 \cdot 2 H_2O$ (Sigma Aldrich, France, >99.9%), $SrCl_2 \cdot 6 H_2O$ (Fluka, Germany, >99%), $BaCl_2 \cdot 2 H_2O$ (Sigma Aldrich, Germany, >99.999%), NaCl (Sigma Aldrich, France, >99.9%) and NaOH (Sigma Aldrich, France) were used as received.

Polymer synthesis. The synthesis of the (block) copolymers was done using reversible addition-fragmentation chain-transfer polymerization and is described in detail in the Supporting Information. The investigated PA-*b*-PSS block copolymers have a block ratio of PA to PSS of 94:6.

Sample preparation. In general the samples were prepared according to a previously suggested approach. The concentration of positive charges is kept constant at 100 mmol L^{-1} . In order to achieve this, the solvent contains 100 mmol L^{-1} NaCl and M^{2+} cations are added by replacing a certain amount of 100 mmol NaCl by the corresponding amount of solution of MCl_2 .

For the scattering experiments, first, an aqueous stock solution of the freeze-dried polymer in 100 mmol L^{-1} NaCl was prepared at a polymer concentration of 8 g L^{-1} and adjusted to pH of 9 using a 100 mmol L^{-1} NaOH solution. The solution is filled up with 100 mmol L^{-1} NaCl solution and the desired amount of 50 mmol L^{-1} $CaCl_2$ ($SrCl_2/BaCl_2$) by drop wise addition under vigorous stirring. The final polymer concentration was 1 g L^{-1} or 4 g L^{-1} .

The samples for SAXS and ITC were prepared in H_2O , otherwise the samples were prepared in D_2O or a mixture of H_2O and D_2O .

Density measurements. The density of the sodium salt of PA and PSS was measured using a DSA 5000 M densitometer (Anton-Paar) in a temperature range from $5 \text{ }^\circ\text{C}$ to $65 \text{ }^\circ\text{C}$. Details can be found in the Supporting Information.

Small angle neutron scattering. SANS measurements were performed at the D11 small angle neutron scattering instrument of the Institut Laue-Langevin (Grenoble, France). Three sample to detector distances (39.0 m collimation 40.5 m, 8.0 m collimation 8.0 m, 1.4 m collimation 5.5 m) and a neutron wavelength of 0.5 nm (FWHM 9%) were used to cover a q-range of $2 \cdot 10^{-2} - 5 \text{ nm}^{-1}$. We used a circular neutron beam with a diameter of 15 mm. Scattered neutrons were detected with a ^3He MWPC detector (CERCA) with 256×256 pixels of $3.75 \text{ mm} \times 3.75 \text{ mm}$ pixel size. The detector images were azimuthally averaged, corrected to transmission of the direct beam and scaled to absolute intensity using a 1 mm H_2O cell as secondary calibration standard ($\frac{d\Sigma}{d\Omega} = 0.929 \text{ cm}^{-1}$) using the LAMP software. The scattering from the solvent and the incoherent background were subtracted from the scattering curves. Details for the data reduction can be found in Chapter 2 of Ref. 34. The sample temperature was adjusted to values between 6 °C to 65 °C using a circulating water bath.

Additional SANS measurements were performed at the KWS2 small angle scattering instrument of the Heinz Maier-Leibnitz Zentrum (Garching, Germany).³⁵ Three sample to detector distances (19.6 m collimation 20.0 m $\lambda = 10 \text{ \AA}$, 7.7 m collimation 8.0 m $\lambda = 5 \text{ \AA}$, 1.7 m collimation 2.0 m $\lambda = 5 \text{ \AA}$) were used to cover a q-range of $3 \cdot 10^{-2} - 1.0 \text{ nm}^{-1}$. Scattered neutrons were detected with a ^3He multitube detector (GE Reuter Stokes Inc).³⁶ The detector images were azimuthally averaged, corrected to transmission of the direct beam and scaled to absolute intensity of plexiglass as secondary calibration standard using the QtiKWS software. The scattering from the solvent and the incoherent background were subtracted from the scattering curves.

Small angle X-ray scattering. Small-angle X-ray scattering experiments were performed at the ID02 beamline of the European Synchrotron Radiation Facility (ESRF). Two sample to detector distances (10 m and 1 m) were measured at a X-Ray energy of 12.46 keV (0.0995 nm) using a Rayonix MX-170HS CCD detector to cover a q-range of $8 \cdot 10^{-3} \text{ nm}^{-1}$ to 6 nm^{-1} .

Additional SAXS data were obtained from the D2AM beamline of the ESRF. Two sam-

ple to detector distances (2.2 m and 0.6 m) were measured at a X-Ray energy of 16.00 keV (0.0775 nm) using a XPAD-D5 hybrid pixel detector to cover a q -range of $5 \cdot 10^{-2} \text{ nm}^{-1}$ to 7 nm^{-1} .

Samples were filled in a 2 mm flow-through quartz glass capillary (WJM Glas Müller, Berlin, Germany) to facilitate accurate background subtraction. The detector images were corrected for dark and flat-field, azimuthally averaged and corrected to transmission of the direct beam. The data were scaled to absolute intensity using water as a secondary standard.^{37,38} Error bars were estimated assuming Poisson statistics.

Static and dynamic light scattering. Static and dynamic light scattering (SLS, DLS) available in the ILL PSCM lab were performed using an ALV CGS-3 (ALV, Langen, Germany) equipped with a HeNe laser operating at $\lambda_0 = 632.8 \text{ nm}$. The samples were filtered in cylindrical quartz glass cells using Millex PDVF filters with a pore size of $0.45 \mu\text{m}$. SLS and DLS were measured simultaneously in an angular range from 30° to 150° in steps of 10°C at temperatures ranging from 6°C to 65°C .

The intensity-time correlation function $g_2(\tau) - 1$ measured with DLS was analyzed using the method of cumulants³⁹

$$g_2(\tau) - 1 = \beta \exp(-2\Gamma\tau) \left(1 + \frac{\mu_2}{2!}\tau^2\right)^2 \quad (3)$$

β is a factor, which depends on the experimental setup, Γ the relaxation rate and μ_2 the second cumulant. The apparent diffusion coefficient $D_{app}(c, q)$ for a given q is calculated according to

$$D_{app} = \frac{\Gamma}{q^2} \quad (4)$$

The diffusion coefficient is extrapolated towards $q = 0$ and where applicable, to $c = 0$ according to^{40,41}

$$D_0 = D_{app}(c, q) (1 + CR_g^2 q^2 + k_D c) \quad (5)$$

where C and k_D are constants describing q and the concentration dependence of D_{app} , respectively. The diffusion coefficient D_0 is used to calculate the hydrodynamic radius R_h using the Stokes-Einstein equation

$$R_h = \frac{k_B T}{6\pi\eta D_0} \quad (6)$$

where T is the temperature, k_B the Boltzmann constant and η the viscosity of the solvent. The temperature dependent viscosity of D₂O, which differs from that of H₂O, was obtained from Ref. 42.

Static light scattering was evaluated with the Zimm equation⁴³

$$\frac{Kc}{\Delta R_\theta} = \frac{1}{M_w} + 2A_2c + \frac{R_g^2}{3M_w}q^2 \quad (7)$$

where c is the mass concentration of the polymer, M_w the weight averaged molar mass of the polymer, A_2 the second osmotic virial coefficient and R_g the radius of gyration. ΔR_θ is the Rayleigh ratio and corresponds to the macroscopic scattering cross-section $\frac{d\Sigma}{d\Omega}$ used to express the scattering intensity in SANS and SAXS. K is the contrast factor given by

$$K = \frac{4\pi^2}{N_A \lambda_0^4} \left(n_{\text{standard}} \frac{dn}{dc} \right)^2 \quad (8)$$

It contains the Avogadro constant N_A , the wavelength of the laser in vacuo λ_0 , the refractive index of the standard (in this case toluene) n_{standard} and the refractive index increment of the polymer in the solvent $\frac{dn}{dc}$.

SLS data were corrected for the scattering from the solvent and normalized to absolute intensities by comparison to a toluene standard.

Small-angle scattering analysis. The form factor fits of the small-angle scattering data were done using the SASET program.⁴⁴ Instrumental resolution for SANS has been taken into account according to Ref. 45. The macroscopic scattering function is convoluted with a resolution function $R(q, \sigma_q)$, which depends on wavelength spread, finite collimation of the

beam and detector resolution

$$\frac{d\Sigma}{d\Omega_{\text{smearred}}}(q) = \int R(q, \sigma_q) \frac{d\Sigma}{d\Omega}(q) dq \quad (9)$$

We took into account the instrumental resolution for all points from each detector configuration and merged the data only for final representation. This approach does not involve truncation of the data in the region of overlapping q , which leads to a larger number of available data points in the analysis.

Scattering for Gaussian and generalized Gaussian chains. The scattering of a Gaussian chain with a radius of gyration R_g and a Flory exponent ν of 0.5 can be described by the Debye equation⁴⁶

$$P(q) = \frac{2 (\exp(-q^2 R_g^2) - 1 + q^2 R_g^2)}{(q^2 R_g^2)^2} \quad (10)$$

In order to be able to describe the scattering from polymer chains where the Flory exponent is deviating from $\nu = 0.5$ the equation can be generalized to⁴⁷

$$P(q) = \frac{1}{\nu U^{\frac{1}{2\nu}}} \gamma\left(\frac{1}{2\nu}, U\right) - \frac{1}{\nu U^{\frac{1}{\nu}}} \gamma\left(\frac{1}{\nu}, U\right) \quad (11)$$

with U being defined as

$$U = (2\nu + 1)(2\nu + 2) \frac{q^2 R_g^2}{6} \quad (12)$$

and $\gamma(a, x)$ the incomplete Gamma function

$$\gamma(a, x) = \int_0^x t^{a-1} \exp(-t) dt \quad (13)$$

Scattering from block copolymer micelles with self-avoiding chains in the corona.

The form factor of self-assembled block copolymers with excluded volume interaction of the polymer chains was first treated by Pedersen.⁴⁸⁻⁵¹ The macroscopic scattering cross-section

$\frac{d\Sigma}{d\Omega}(q)$ of a solution of block copolymer micelles can be written as⁵⁰

$$\begin{aligned} \frac{d\Sigma}{d\Omega}(q) = N & \left[N_{\text{agg}}^2 \beta_{\text{core}}^2 A_{\text{core}}^2(q) + N_{\text{agg}} \beta_{\text{corona}}^2 P'_{\text{corona}}(q) \right. \\ & \left. + 2N_{\text{agg}}^2 \beta_{\text{core}} \beta_{\text{corona}} A_{\text{core}}(q) A_{\text{corona}}(q) + N_{\text{agg}} (N_{\text{agg}} - P'_{\text{corona}}(0)) \beta_{\text{corona}}^2 A_{\text{corona}}^2(q) \right] \end{aligned} \quad (14)$$

where N is the number density of micelles, N_{agg} the aggregation number of micelles, β_{core} and β_{corona} are the total excess scattering length of the block forming the spherical core and the corona, respectively. They are defined as

$$\beta_{\text{corona}} = V_{\text{m, corona}} \text{DP}_{\text{corona}} \Delta\rho_{\text{corona}} \quad (15)$$

and

$$\beta_{\text{core}} = V_{\text{m, core}} \text{DP}_{\text{core}} \Delta\rho_{\text{core}} \quad (16)$$

with V_{m} being the molecular volume of the respective monomer unit, $\text{DP}_{\text{corona}}$ and DP_{core} the degree of polymerization of the corona and core block and $\Delta\rho$ the corresponding excess scattering length density.

Equation 14 consists of four different contributions: scattering from the spherical and homogeneous core $A_{\text{core}}^2(q)$, scattering from the polymer chains in the corona $P'_{\text{corona}}(q)$, the cross-term between core and corona $A_{\text{core}}(q) \cdot A_{\text{corona}}(q)$ and the cross-term between different chains $A_{\text{corona}}^2(q)$. $A_{\text{core}}(q)$ is the scattering amplitude of a homogeneous sphere⁵² with radius R_{core}

$$A_{\text{core}}(q) = 3 \frac{\sin(qR_{\text{core}}) - qR_{\text{core}} \cos(qR_{\text{core}})}{(qR_{\text{core}})^3} \quad (17)$$

$P'_{\text{corona}}(q)$ is the form factor of a chain in the corona. It contains the self-correlation of the chain $P_{\text{exv}}(q)$ as well as the interaction between the chains, which is expressed by the interaction parameter ν ^{50,53}

$$P'_{\text{corona}}(q) = \frac{P_{\text{exv}}(q)}{1 + \nu P_{\text{exv}}(q)} \quad (18)$$

where $P_{\text{exv}}(q)$ is the form factor of a semi flexible self-avoiding chain, which is characterized

by a radius of gyration of the polymer chains in the corona $R_{g,\text{corona}}$. This form factor was first derived by Pedersen and Schurtenberger⁵⁴ and later corrected⁵⁵. In experiments ν typically adopts values between 0 and 8 and is related to the osmotic compressibility κ by^{50,53,56}

$$\kappa = 1 + \nu \quad (19)$$

$A_{\text{corona}}(q)$ is given by

$$A_{\text{corona}}(q) = \frac{\int \rho_{\text{corona}}(r) r^2 \frac{\sin(qr)}{qr} dr}{\int \rho_{\text{corona}}(r) r^2 dr} \quad (20)$$

with $\rho_{\text{corona}}(r)$ as the scattering length density profile in the corona. In this work we use a Gaussian profile, which is defined as

$$\rho_{\text{corona}}(r) = \begin{cases} 0 & \text{for } r < R_{\text{core}} \\ 1 & \text{for } r = R_{\text{core}} \\ \exp\left(\frac{-(r-R_{\text{core}})^2}{2s^2}\right) & \text{for } r > R_{\text{core}} \end{cases} \quad (21)$$

with s controlling the thickness of the corona.

In order to take into account the size distribution of micelles we assumed a log-normal distribution of the aggregation number N_{agg}

$$p(N_{\text{agg}}) = \frac{1}{H\sqrt{2\pi}N_{\text{agg}}} \exp\left(\frac{-\log(N_{\text{agg}} - M)^2}{2H^2}\right) \quad (22)$$

where H and M define the distribution and are connected to the mean aggregation number $\overline{N_{\text{agg}}}$ and standard deviation $\sigma_{\overline{N_{\text{agg}}}}$ by

$$\overline{N_{\text{agg}}} = \exp\left(M + \frac{H^2}{2}\right) \quad (23)$$

$$\sigma_{\overline{N_{\text{agg}}}} = \sqrt{\exp(H^2 + 2M) (\exp(H^2) - 1)} \quad (24)$$

The macroscopic scattering cross-section is therefore

$$\frac{d\Sigma}{d\Omega}_{\text{polydisperse}}(q) = \int \frac{d\Sigma}{d\Omega}(q)p(N_{\text{agg}})dN_{\text{agg}} \quad (25)$$

Isothermal titration calorimetry. ITC measurements were performed using a VP-ITC from Malvern Instruments. Typically, the cell contained 1.4 mL of polymer solution and the injection volumes were increased continuously during the titration ranging from 3 μL to 16 μL with a time span of 300 s in between the injections. In order to avoid the “first injection anomaly”, a short down motion of the plunger was performed prior to insertion of the syringe into the active chamber.⁵⁷ A wider range of M^{2+} /polymer ratios was covered by performing several titrations with changing concentration of earth alkaline metal cations.⁵⁸ The baseline correction and integration was performed using NITPITC.⁵⁹ We did not correct the signals for the heat of dilution of the polyelectrolyte and the metal cations since those contributions were considerably smaller than the heat of binding. The data were, if possible, fitted using the model of a single set of identical sites or two sets of independent sites. The details of the models are described in the Supporting Information.

Results and discussion

Solution behavior. We showed previously that aqueous solutions of PA-*b*-PSS block copolymers form spherical block copolymer micelles in the presence of Ca^{2+} . Since Ca^{2+} shows a specific interaction with PA but not with PSS, Ca^{2+} complexes the PA block and forms the core of the micelles, while PSS forms the corona. Furthermore, we demonstrated that micelle formation can be triggered for a sample in the single chain state by an increase of temperature due to the entropic nature of the Ca^{2+} binding to PA.²⁰

Table 1: Overview of polymer composition, weight-averaged molecular weight M_w and hydrodynamic radius R_h determined from NMR and static and dynamic light scattering in 100 mmol L⁻¹ NaCl and in the absence of M^{2+} .

Sample	PA:PSS /mol % ^a	M_w /kg mol ^{-1b}	R_h /nm ^c
h ₃ -PA ₁₁₉₀ PSS ₇₀	94:6	160 ± 2	13.8 ± 0.6
d ₃ -PA ₁₁₉₀ PSS ₇₀	94:6	181 ± 3	13.6 ± 0.5

Obtained by ^a NMR, ^b SLS and ^c DLS.

The main focus of this work is to clarify if similar micelles can be found for the two other earth alkaline cations Sr^{2+} and Ba^{2+} and in particular how temperature changes affect the binding of the multivalent cations to the block copolyelectrolyte. For the present work we choose a polymer with a long PA block and a relatively short PSS block. In order to exploit the full potential of SANS we use a blockcopolymer which contains a deuterated polyacrylate block. Deuteration allows us to match different parts of the polymer in neutron scattering by using mixtures of light and heavy water as a solvent.⁶⁰ The corresponding polymer is denoted as d₃-PA₁₁₉₀PSS₇₀. In addition, we use an identical block copolymer with fully hydrogenated blocks, denoted as h₃-PA₁₁₉₀PSS₇₀. Figure 1A shows the chemical structure of the block copolymers and Table 1 summarizes the molecular weights and hydrodynamic radii from DLS/SLS as well as the ratio between PA and PSS of the block copolymers determined by NMR. Details of the characterization can be found in Ref. 20 and in the Supporting Information.

In order to facilitate meaningful scattering experiments and suppress potential inter-

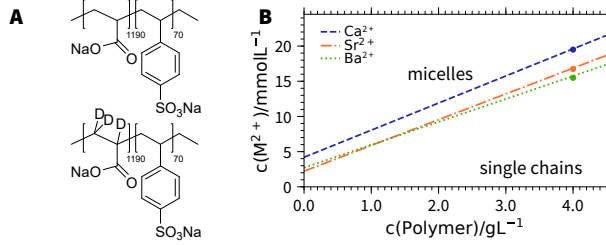


Figure 1: **A** Chemical structure of the block copolymers. **B** Simplified diagram of micelle formation with d_3 -PA₁₁₉₀PSS₇₀/ h_3 -PA₁₁₉₀PSS₇₀ in the presence of Ca²⁺, Sr²⁺ and Ba²⁺. The points indicate the compositions, where temperature dependent SANS and light scattering experiments were performed. An extended version of the phase diagram can be found in the Supporting Information.

particular interferences by electrostatic screening, all experiments were performed in the presence of additional NaCl as an inert salt. Addition of NaCl was limited to accomplish an overall level of cationic charges of $0.1 \text{ M} = 2[M^{2+}] + [\text{Na}^+]$. Variation of this level would have generated one further parameter to control the interactions,^{24,61} but was not applied in the present work to keep the complexity as low as possible. Figure 1B illustrates the solution behavior of h_3 -PA₁₁₉₀PSS₇₀/ d_3 -PA₁₁₉₀PSS₇₀ in the presence of Ca²⁺, Sr²⁺ and Ba²⁺ at room temperature. The boundaries for micelle formation with h_3 -PA₁₁₉₀PSS₇₀ and d_3 -PA₁₁₉₀PSS₇₀ are identical within the experimental accuracy. The block copolymer shows a solution behavior, which is similar to the one observed for PA homopolymers described by eq 1. This means that with increasing polymer concentration the amount of M^{2+} required to induce a phase transition increases. However, instead of a precipitation as found for PA homopolymers,^{25,61,62} the formation of stable micelles takes place in the case of block copolyelectrolytes.

In order to investigate the structure of the micelles in the presence of Ca²⁺, Sr²⁺ and Ba²⁺ we performed SAXS experiments of h_3 -PA₁₁₉₀PSS₇₀ in the micelle regime in the presence of the three cations. Figure 2 shows the corresponding SAXS profiles of a sample in the single chain region and in the micelle region for all three cations, respectively.

The curve with the lowest concentration of M^{2+} shows a slope close to -2 at high q . Upon increase of the M^{2+} concentration a dramatic increase of the forward scattering is

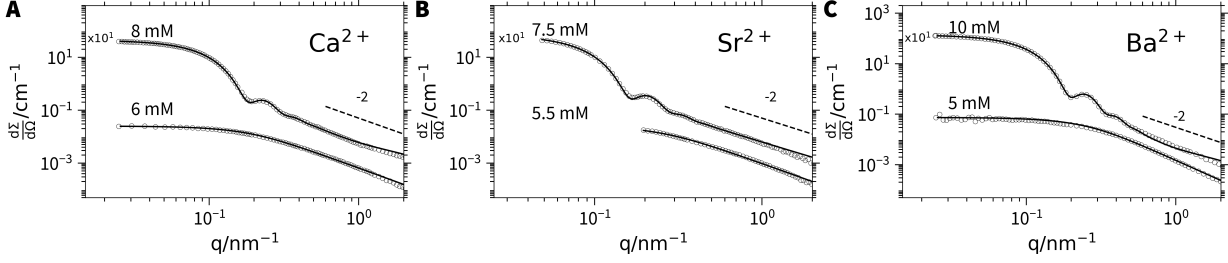


Figure 2: SAXS profiles of $h_3\text{-PA}_{1190}\text{PSS}_{70}$ ($c = 1 \text{ g L}^{-1}$) in the presence of different concentrations of Ca^{2+} (A), Sr^{2+} (B) and Ba^{2+} (C). The solid lines represent fits to the model of generalized Gaussian chain⁴⁷ or a spherical polydisperse block copolymer micelle.^{48,50} Table 2 summarizes the results of the fits.

observed together with the formation of well-defined minima in the scattering curves. This shows that block copolymer micelles are formed in the presence of all three cations.

The curves in the single chain region can be well described by the model of a generalized Gaussian chain⁴⁷ with Table 2 summarizing the fit parameters. The resulting radii of gyration $R_{g,\text{free}}$ range between 6.3 nm and 8.2 nm. Moreover, we find Flory exponents ν between 0.4 and 0.5, which is close to the value of polymers in a θ solvent. We do not observe a structure factor, which implies that the charges of the polyelectrolytes are highly screened due to the large amount of salt present in solution.

Table 2: Structural parameters from the form factor fits of the SAXS data shown in Figure 2. An extended version including errors of the fitting parameters can be found in the Supporting Information. Fits at the lower $c(\text{M}^{2+})$ were carried out with the model of generalized Gaussian chains⁴⁷ and fits at the higher $c(\text{M}^{2+})$ with the model of a spherical block copolymer micelle^{20,48,50} or a mixture of block copolymers and free generalized Gaussian chains.

	Ca^{2+}		Sr^{2+}		Ba^{2+}	
$c(\text{M}^{2+})/\text{mM}$	6	8	5.5	7.5	5	10
ϕ_{micelles}	0.0	0.79	0.0	0.73	0.0	1.0
$R_{g,\text{free}}/\text{nm}$	8.2	5.2	6.3	6.2	6.7	—
ν	0.49	0.36	0.44	0.53	0.38	—
$R_{\text{core}}/\text{nm}$	—	22.8	—	25.6	—	21.6
$\frac{\sigma_{R_{\text{core}}}}{R_{\text{core}}}$	—	0.109	—	0.104	—	0.113
$R_{g,\text{corona}}/\text{nm}$	—	0.7	—	2.3	—	1.0
f_{solvent}	—	0.83	—	0.60	—	0.90

We used the previously suggested model of spherical block copolymer micelles,^{20,48,50} consisting of a PA core complexed by the multivalent cation M^{2+} and PSS chains in the corona to describe the data of the samples in the micelle region. This model has been shown to describe the situation for Ca^{2+} and is expected to be similar for all three cations as the binding to PA is similar and the PA block is considerably longer than the PSS block. The fit parameters are summarized in Table 2. The scattering curves for the micelles formed in the presence of all three cations can be well described by the suggested model. The micelles have similar dimensions, consisting of a relatively large core formed of PA/ M^{2+} with a radius R_{core} between 21.6 and 25.6 nm. The corona is formed by PSS and is rather thin with a radius of gyration of the polymers in the corona $R_{g, \text{corona}}$ between 0.7 and 2.3 nm. The overall micelles are rather monodisperse with polydispersities $\frac{\sigma_{R_{\text{core}}}}{R_{\text{core}}}$ close to 10%. By fitting the scattering data in absolute intensities, knowing the polymer concentration, scattering length densities and block lengths it turned out that the micelle cores contain a large volume fraction f_{solvent} of water. f_{solvent} is defined as

$$f_{\text{solvent}} = 1 - \frac{\left(V_{\text{m, monomer unit}} + 0.5V_{\text{m, M}^{2+}} \right) \text{DP}_{\text{core}} N_{\text{agg}}}{\frac{4}{3}\pi R_{\text{core}}^3} \quad (26)$$

where $V_{\text{m, monomer unit}}$ is the molecular volume of one monomer unit of the core forming block in this case PA and $V_{\text{m, Ca}^{2+}}$ the molecular volume of the corresponding divalent cation, DP_{core} the degree of polymerization of the core block and N_{agg} the aggregation number. The high volume fractions of water found for the core of the micelles are in agreement with our previous contrast-variation study of PA-*b*-PSS in the presence of Ca^{2+} .²⁰

For the micelles in the presence of Ca^{2+} and Sr^{2+} we had to take into account a small fraction of non-micellized polymer chains ($\phi_{\text{micelles}} < 1.0$).

Since Ba^{2+} also interacts with the PSS block we also tried a model with Ba^{2+} /PSS in the core of the micelles and PA in the corona. The polymer concentration, knowledge of block length and the corresponding molar volumes of the blocks allowed us to heavily constrain

the fit. This model was not able to describe the data sufficiently well and furthermore gave unreasonable values for the parameter s controlling the corona thickness and the radius of gyration of the polymers in the corona $R_{g,\text{corona}}$. The best fit is shown in Figure S8.

In short, we find spherical micelles with similar dimensions for Ca^{2+} , Sr^{2+} and Ba^{2+} . The core of the micelles are formed by PA/ M^{2+} together with a high volume fraction of water. The corona of the micelles is formed by PSS. PA is complexed by the multivalent cation and therefore a microphase separation of the M^{2+} /PA blocks is taking place. The complex forms the core of the micelle and is highly swollen with water, typical for liquid-liquid phase transitions.²⁰ PSS forms the corona of the micelles and stabilizes the aggregates by charge repulsion.

Temperature effect on the phase behavior. In order to study the effect of temperature on the self-assembly of the block copolymer in the presence of earth alkaline cations we choose points in the phase diagram which are close to the single chain to micelle transition indicated as dots in Figure 1B. Since we also performed SANS measurements on those samples we used the block copolymer $\text{d}_3\text{-PA}_{1190}\text{PSS}_{70}$. At room temperature all of these samples are considered to be in the single chain state. We performed temperature dependent DLS and SLS on these samples. Figure 3 shows the hydrodynamic radii R_h and the apparent molecular weight $M_{w,\text{app}}$ obtained from the temperature dependent light scattering measurements.

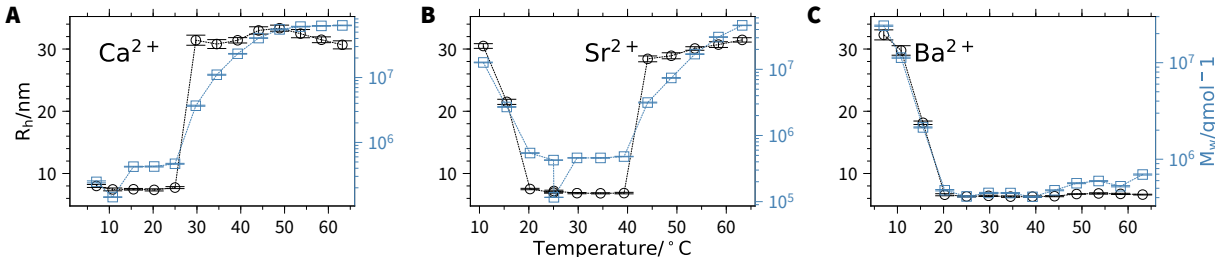


Figure 3: Hydrodynamic radius R_h and apparent molecular weight $M_{w,\text{app}}$ of $\text{d}_3\text{-PA}_{1190}\text{PSS}_{70}$ in the presence of Ca^{2+} (A), Sr^{2+} (B) and Ba^{2+} (C) as a function of temperature. The lines are guide to the eyes. The polymer concentration is 4 g L^{-1} . The concentration of M^{2+} is: Ca^{2+} 19.5 mmol L^{-1} , Sr^{2+} 16.75 mmol L^{-1} , Ba^{2+} 15.5 mmol L^{-1} . The solvent is composed of 25.2% D_2O .

Figure 3A shows the results for the block copolyelectrolyte in the presence of Ca^{2+} . The hydrodynamic radius at low temperatures (6 °C to 25 °C) is close to 8 nm, which we attribute to the presence of single chains of block copolymers in solution. Above 25 °C R_h increases to around 30 nm. Similarly, the apparent molecular weight $M_{w,\text{app}}$ increases from $4 \cdot 10^5 \text{ g mol}^{-1}$ to $6 \cdot 10^7 \text{ g mol}^{-1}$. We attribute this strong increase to the formation of block copolymer micelles. It has been shown previously for PA homopolymers that an increase in temperature can be used to promote binding of Ca^{2+} to the polyelectrolyte chain.²⁶ This results in a chain collapse and eventually in aggregation and precipitation of the polymer. As demonstrated in our previous work,²⁰ stronger binding of Ca^{2+} to the PA block leads to microphase separation due to the same temperature promoted binding of Ca^{2+} to PA. A detailed analysis of the structure using small-angle neutron scattering confirming this feature is presented later. We performed temperature cycles with the same sample several times and found that the temperature induced single-chain to micelle transition was highly reproducible.²⁰

Figure 3B shows R_h and $M_{w,\text{app}}$ as a function of temperature for the PA-*b*-PSS block copolymer in the presence of Sr^{2+} . Again, a hydrodynamic radius of around 8 nm and an apparent molecular weight of $4 \cdot 10^5 \text{ g mol}^{-1}$ indicates the presence of single chains in solution at room temperature. Upon increase of the temperature above 40 °C a strong increase of R_h as well as $M_{w,\text{app}}$ occurs similar to the increase observed with Ca^{2+} cations. However, at temperatures below 20 °C R_h and $M_{w,\text{app}}$ also increase. From this we conclude that block copolymer micelles are formed at high as well as low temperatures with an intermediate region where the polymers are present as single chains. A previous work already showed that an increase of temperature promotes the binding of Ca^{2+} and Sr^{2+} to PA due to the entropic nature of the complexation.²⁶ However, lowering the temperatures did not show a chain collapse or aggregation of PA homopolymers. Even though PSS does not show a precipitation threshold with Sr^{2+} we hypothesize that the PSS block plays an important role in the formation of the micelles at low temperatures. In order to shed light onto the

binding situation we will use SANS and isothermal titration calorimetry experiments.

Figure 3C shows the results for the block copolymer in the presence of Ba^{2+} . In contrast to the samples with Ca^{2+} , there is an increase in R_h and $M_{w,\text{app}}$ at low temperatures comparable to the sample with Sr^{2+} . Both quantities show a value close to the typical value of single chains at 25 °C. From this we conclude that micelles are formed at low temperatures, while at temperatures in the regime of $20^\circ\text{C} < T < 40^\circ\text{C}$ the sample contains single chains.

Thermodynamics of cation binding and micelle formation. In order to gain further insight into the origin of the described temperature behavior we used isothermal titration calorimetry (ITC) to link the information we obtained from temperature dependent light scattering with thermodynamic quantities. ITC allows us to measure the consumed or released heat upon addition of M^{2+} to a solution of polyelectrolyte for a given temperature. The measured heat can be attributed to the binding of the metal cation to the anionic moiety.

There are several driving forces for the binding of multivalent cations and micelle formation which have to be taken into account. The binding of multivalent cations to the anionic moiety results in a gain in entropy since two Na^+ are replaced by one M^{2+} . A release of water molecules from hydration shells also results in a gain of entropy. Equally important, the enthalpy of binding has to be taken into account.

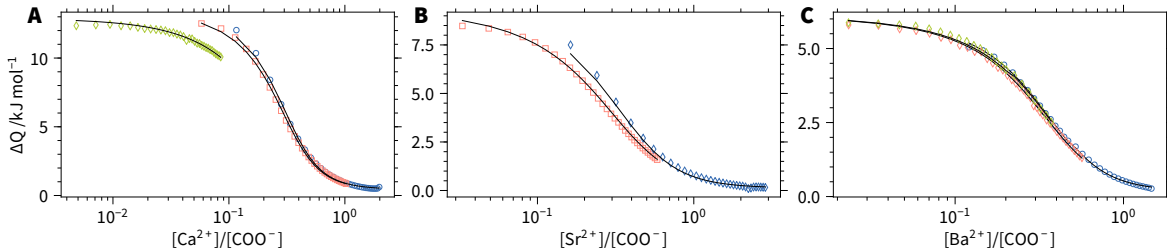


Figure 4: Isothermal titration curve of PA in the presence of Ca^{2+} (A), Sr^{2+} (B) and Ba^{2+} (C). The curves show the heat of binding per injection as a function of the M^{2+}/PA ratio. We performed several titrations with varying concentrations of M^{2+} to cover a large range of M^{2+}/PA . The solid lines are global fits with the model of a single set of identical binding sites. Details can be found in the Supporting Information. Table 3 summarizes the results.

In order to compare the contributions from the PA and PSS blocks we performed ITC

experiments on PA and PSS homopolymers in the presence of the three earth alkaline metal cations. Figure 4 shows the titration curves of PA with the three investigated earth alkaline metal cations at 25.0 °C. The heat of binding ΔQ is positive for all cations and follows a sigmoidal curve. This indicates that the binding of M^{2+} to PA is an endothermic process. We performed several titrations with varying concentrations of M^{2+} in the syringe to access a larger range of M^{2+}/PA . The data can be described by the model of a single set of identical binding sites, which is described in detail in the Supporting Information. All titrations for a given combination of M^{2+} were analyzed globally using the same fitting parameters. Table 3 summarizes the results of the data analysis.

Table 3: Thermodynamic data for the M^{2+} binding to PA and PSS from ITC at 25 °C.

Polymer	M^{2+}	$K /L mol^{-1}$	$\Delta H /kJ mol^{-1}$	$T\Delta S /kJ mol^{-1}$	$\Delta G /kJ mol^{-1}$	n
PA	Ca^{2+}	$5.60 \cdot 10^3 \pm 0.16 \cdot 10^3$	16.3 ± 0.2	37.7 ± 0.3	-21.4 ± 0.1	0.264 ± 0.002
PA	Sr^{2+}	$3.68 \cdot 10^3 \pm 0.21 \cdot 10^3$	13.4 ± 0.4	33.8 ± 0.5	-20.4 ± 0.1	0.266 ± 0.005
PA	Ba^{2+}	$4.99 \cdot 10^3 \pm 0.16 \cdot 10^3$	7.6 ± 0.1	26.2 ± 0.2	-21.1 ± 0.1	0.321 ± 0.002
PSS	Ca^{2+}	$2.82 \cdot 10^2 \pm 0.19 \cdot 10^2$	4.3 ± 0.4	18.3 ± 0.6	-14.0 ± 0.2	0.228 ± 0.016
PSS	Sr^{2+} (I)	$5.13 \cdot 10^3 \pm 2.91 \cdot 10^3$	2.2 ± 0.2	19.0 ± 1.8	-21.2 ± 1.4	0.187 ± 0.008
	Sr^{2+} (II)	$4.27 \cdot 10^2 \pm 2.83 \cdot 10^2$	-0.23 ± 0.61	14.8 ± 1.7	-15.0 ± 1.6	2.156 ± 0.160

From the fits we obtain the enthalpy of binding ΔH , entropy of binding ΔS , binding constant K and the binding stoichiometry n . We find a positive binding enthalpy for all three cations demonstrating that the binding of M^{2+} to PA is driven by entropy for all three metal cations. In a previous work²⁸ on PA and Ca^{2+} this gain of entropy has been attributed to the release of two sodium cations as well as several water molecules upon binding. Compared to this previous work, we find slightly smaller binding enthalpies which we attribute to the presence of NaCl in our experiments compared to pure water. In fact, an increase in ionic strength in the solution leads to a decrease in ΔH for the binding of multivalent cations to DNA.⁶³ The binding enthalpy ΔH and along with it the entropy of binding ΔS decreases according to $Ca^{2+} > Sr^{2+} > Ba^{2+}$. We attribute the decrease of ΔS when going from Ca^{2+} , Sr^{2+} and Ba^{2+} to a decreased amount of water released from hydration shells upon binding.

Next, we performed titration experiments for a PSS homopolymer in the presence of the three metal cations. Figure 5 shows the corresponding titration curves. For Ca^{2+} the curves

can be well described by the model of a single set of identical binding sites with a positive binding enthalpy. Compared to Ca^{2+}/PA the binding enthalpy ΔH , entropy ΔS as well as the binding constant K are considerably smaller for $\text{Ca}^{2+}/\text{PSS}$. Table 3 summarizes the results from the data analysis. The smaller binding constant K is in agreement with the macroscopic observation, that there is no phase separation for PSS in the presence of Ca^{2+} .

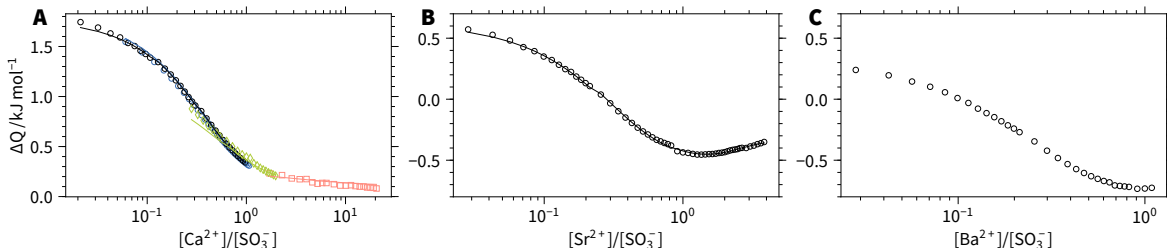


Figure 5: Isothermal titration curve of PSS in the presence of Ca^{2+} (A), Sr^{2+} (B) and Ba^{2+} (C). The curves show the heat of binding per injection as a function of the M^{2+}/PA ratio. We performed several titrations for Ca^{2+} with varying concentrations of polymer to cover a large range of $\text{Ca}^{2+}/\text{PSS}$. The solid lines are global fits with the model of a single set of identical binding sites (A) and two sets of independent sites (B). Details can be found in the Supporting Information. Table 3 summarizes the results of the data analysis

Figure 5B shows the titration curve of $\text{Sr}^{2+}/\text{PSS}$. The curve differs considerably from the one found for $\text{Ca}^{2+}/\text{PSS}$. Clearly, there are two processes occurring upon addition of Sr^{2+} to PSS: First, a binding process with a positive ΔH is taking place at low $\text{Sr}^{2+}/\text{PSS}$ ratios. This is followed by a second process which has a negative ΔH contribution. Similarly, we find a two step binding process for the titration of Ba^{2+} to PSS, where again the first binding process has a positive ΔH contribution and the second process has a negative one.

A previous work²⁹ already revealed this two step process for the $\text{Ba}^{2+}/\text{PSS}$ system. In a first step, two Na^+ cations are replaced per Ba^{2+} entering the polyelectrolyte domains, which results in a gain of entropy ΔS and a positive ΔH contribution. At higher M^{2+}/PSS ratios the actual binding of the metal cation to the polyelectrolyte chain takes place as a second step with a negative ΔH term. From a qualitative comparison of the two curves in Figure 5B and C it is obvious that this second contribution is weaker for Sr^{2+} than for

Ba^{2+} . This is in agreement with the macroscopic phase behavior. Whereas the system $\text{Sr}^{2+}/\text{PSS}$ shows no precipitation threshold at 25 °C, $\text{Ba}^{2+}/\text{PSS}$ does show one. We tried to fit the data with the model of two independent binding sites, which was successful for Sr^{2+} . However, for Ba^{2+} using this model was not successful, which we mostly attribute to the smaller accessible M^{2+}/PSS range compared to Sr^{2+} due to the precipitation of $\text{Ba}^{2+}/\text{PSS}$ from solution at the end of the titration. This makes the data at high $\text{Ba}^{2+}/\text{PSS}$ ratios unusable. The result of the fit for $\text{Sr}^{2+}/\text{PSS}$ are summarized in Table 3. The obtained values confirm that two successive binding processes, one with positive ΔH and one with negative ΔH , occur. The same two successive binding processes occur with alkaline earth cations and PA. They are however more difficult to be discerned as both processes are endothermic.

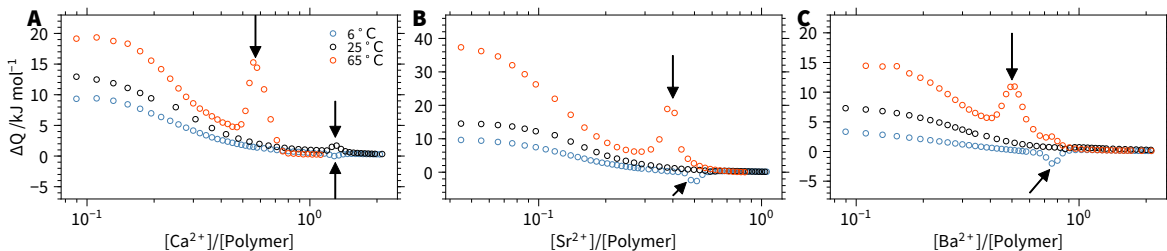


Figure 6: Isothermal titration curve of $\text{h}_3\text{-PA}_{1190}\text{PSS}_{70}$ in the presence of Ca^{2+} (A), Sr^{2+} (B) and Ba^{2+} (C) at 6 °C, 25 °C and 65 °C. The curves show the heat of binding per injection as a function of the $\text{M}^{2+}/\text{monomer unit}$ ratio.

After elucidating the effect of earth alkaline metal cations on the PA and PSS homopolymers we performed ITC measurements on the $\text{h}_3\text{-PA}_{1190}\text{PSS}_{70}$ block copolymer system. As the length of the PA block is much longer than the length of the PSS block we expect the ITC experiments to be dominated by the binding of M^{2+} to the PA block. Figure 6A shows the titration curves with Ca^{2+} at 6 °C, 25 °C and 65 °C. The titration curves are composed of two parts: The first part, which shows that heat is consumed upon addition of M^{2+} resembles the binding curves observed for M^{2+} to PA. The second part consists of a peak at higher $\text{M}^{2+}/\text{polymer}$ ratios. The peak at 25 °C corresponds to the sample composition where micellization was observed (Figure 1B), which is also an endothermic process and hence driven by entropy. We marked the micellization peaks for all curves with an arrow.

When decreasing the temperature the heat consumed upon addition of Ca^{2+} decreases, in agreement with the entropy driven binding of Ca^{2+} to PA. A decrease in temperature reduces the term $T\Delta S$ and consequently ΔH becomes smaller in order to get similar values for the free energy ΔG . Furthermore, when the temperature is lowered the height of the micellization peak decreases. At 6°C the peak nearly disappears.

Figure 6B shows titration curves with Sr^{2+} at 6°C , 25°C and 65°C . Similar as for Ca^{2+} the first part of the titration curve shows positive values for ΔQ and resembles the binding of Sr^{2+} to PA. At higher Sr^{2+} /polymer ratios we again observe a micellization peak. At 65°C the same positive peak appears and disappears at 25°C as observed in case of Ca^{2+} . However, the titrations at 6°C with Sr^{2+} revealed a noticeable difference from the respective results observed in the presence of Ca^{2+} as a small negative peak occurs at high Sr^{2+} /polymer ratios. The ITC experiments carried out with the PSS homopolymer and Sr^{2+} suggest that the negative peak at 6°C might arise from the second binding process of Sr^{2+} to PSS which has a negative sign. Since the PSS block is considerably shorter than the PA block the signal arising from binding of Sr^{2+} is expected to be weak resulting in a very small contribution, which becomes more pronounced at low temperatures.

Figure 6C shows titration curves with Ba^{2+} at 6°C , 25°C and 65°C . Again, we find a decrease of the initial values of ΔQ with decreasing temperature. Similarly as for Sr^{2+} we find a positive peak at high temperatures and a negative peak at low temperatures. Applying the same argument used already for Sr^{2+} we could expect the negative contribution arising from the second binding step of Ba^{2+} to PSS.

A quantitative comparison of the titration curves of the block copolyelectrolytes with those of the respective homopolymers shown in Figure 5B and 5C also explains why the negative peak of the second process in the case of Ba^{2+} /PSS binding has a more negative ΔH term than the negative peak of the Sr^{2+} /PSS binding. Moreover, the binding enthalpy of Ba^{2+} /PA during the initial period of titration is smaller than the one for Sr^{2+} /PA.

We believe that a subtle balance of all these individual contributions results in the ob-

served temperature behavior. We conclude that binding of Sr^{2+} and Ba^{2+} to the PSS block promotes the formation of micelles at low temperatures with PSS in the core since it makes the PSS block more hydrophobic, while the PA block becomes more hydrophilic.

Invertible micelles as seen by SANS In order to get a more detailed insight into the structures of the micelles we performed temperature dependent SANS for the three in Figure 3 discussed samples. The use of a deuterated PA block allowed us to match out the scattering from the PSS block. Accordingly, use of a mixture of 74.8 % light and 25.2 % heavy water as solvent results in a scattering contrast where the scattering from $\text{d}_3\text{-PA}$ is dominating while the scattering from PSS is very weak. This facilitates the investigation of the micellar structure since the scattering patterns allow easily to distinguish between a model of PA forming the core or the corona. Figure 7 shows the SANS profiles for $\text{d}_3\text{-PA}_{1190}\text{PSS}_{70}$ in the presence of Ca^{2+} (A), Sr^{2+} (B) and Ba^{2+} (C) at distinct temperatures. For all samples we choose 8°C and 65°C as temperatures. For the sample with Sr^{2+} we additionally performed a SANS measurement at 25°C .

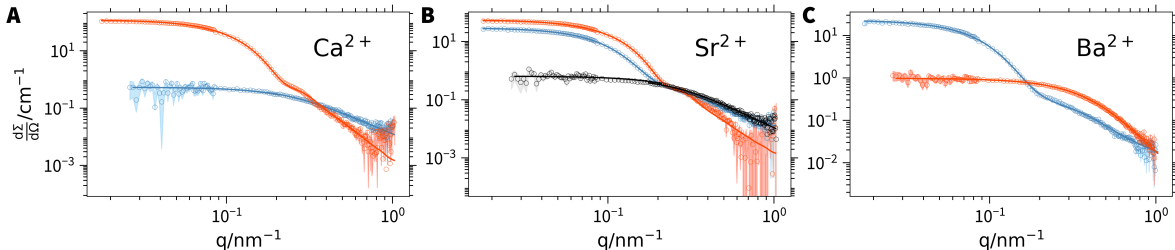


Figure 7: SANS profiles of $\text{d}_3\text{-PA}_{1190}\text{PSS}_{70}$ in the presence of Ca^{2+} , Sr^{2+} and Ba^{2+} at 8°C (blue), 25°C (black) and 65°C (red). The solvent is composed of 25.2 % D_2O . The samples are identical to the ones in Figure 3. The solid lines represent fits to the model of a generalized Gaussian chain⁴⁷ or block copolymer micelles.^{48,50} Table 4 summarizes the resulting fit parameters.

The blue curve in Figure 7A shows the SANS profile of $\text{d}_3\text{-PA}_{1190}\text{PSS}_{70}$ in the presence of Ca^{2+} at 8°C . The curve shows a slope close to -2 at high q and has no distinct oscillations. The curve can be well described by the form factor of a generalized Gaussian chain⁴⁷ with a radius of gyration $R_{g,\text{free}}$ of 6.9 nm and a Flory exponent ν of 0.4. Table 4 summarizes the

hydrodynamic radius from DLS and the $R_{g,\text{free}}$ and ν obtained from the form factor analysis of the SANS data. Hence, the block copolymers exist as single chains in solution at low temperatures in the presence of Ca^{2+} .

The red curve in Figure 7A shows the SANS profile at 65 °C. Compared to the curve at low temperatures the forward scattering is higher and there is a characteristic oscillation at around $q = 0.22 \text{ nm}^{-1}$. At high q we find a slope considerably steeper, indicating a compacter morphology of the polyacrylate chain at high temperatures. From the Guinier analysis at low momentum transfer q we obtain a radius of gyration of 16.7 nm. Based on this and the previous results²⁰ we used the model of a polydisperse block copolymer micelle to describe the data.^{48,50} This model assumes that PA complexed by Ca^{2+} forms the core of the micelle, while the corona is formed by PSS. In order to get reliable results for the aggregation number and the structure we heavily constrained the fit using the known block ratio, molar volumes, polymer concentration and scattering length densities.²⁰ Details can be found in the Supporting Information. The red solid line in Figure 7A shows the best fit with this model. Table 4 summarizes the fit parameters. We obtain an aggregation number of 145 together with a core radius of 17.6 nm. Moreover, we find a radius of gyration for the PSS blocks in the corona of $1.0 \pm 1.0 \text{ nm}$, which is close to the value we found in a previous study using the same polymer.²⁰ Recovery of this finite size for the value of $R_{g,\text{corona}}$ can be attributed to the fact that there is a slight mismatch of the scattering length density of the solvent. One also should keep in mind the large error bar of this parameter, which indeed shows that the scattering from the corona is very weak. In a previous work²⁰ we investigated the micelle structure deep in the micelle regime in the presence of Ca^{2+} at 25 °C. Compared to this previous work, the micelles formed with Ca^{2+} at 65 °C (Figure 7A) contain a slightly lower amount of water. We attribute this lower water content to a larger amount of released water molecules from the PA/Ca^{2+} . This is in agreement with the ITC measurements, which showed that the binding is driven by entropy which mainly arises from the release of water molecules, getting more pronounced at high temperatures.

Table 4: Structural parameters from the form factor fits of the SANS data shown in Figure 7 for d_3 -PAA₁₁₉₀PSS₇₀ in a solvent containing 25.2% D₂O. An extended version including error estimates can be found in the Supporting Information.

	Ca ²⁺		Sr ²⁺			Ba ²⁺	
	8 °C	65 °C	8 °C	25 °C	65 °C	8 °C	65 °C
Temperature	8 °C	65 °C	8 °C	25 °C	65 °C	8 °C	65 °C
R_h^a	8.0	30.7	30.5	7.2	31.5	29.8	6.6
R_g^b	6.3	16.7	21.6	6.5	19.8	20.7	4.7
$R_{g,free}$	6.9	—	—	6.7	—	—	5.0
ν	0.40	—	—	0.37	—	—	0.26
Micelle core	—	PA/Ca ²⁺	PSS/Sr ²⁺	—	PA/Sr ²⁺	PSS/Ba ²⁺	—
N_{agg}	—	145	38	—	81	36	—
R_{core}	—	17.6	7.0	—	18.3	5.6	—
$\frac{\sigma_{R_{core}}}{R_{core}}$	—	0.19	0.10	—	0.17	0.02	—
$R_{g,corona}$	—	1.0	9.8	—	1.2	8.0	—
$f_{solvent}$	—	0.650	0.669	—	0.705	0.707	—

^a Obtained from DLS. ^b Obtained from Guinier analysis of the SANS data.

Figure 7B shows SANS profiles of d_3 -PAA₁₁₉₀PSS₇₀ in the presence of Sr²⁺ at a temperature of 8 °C, 25 °C and 65 °C. The black curve shows the sample at 25 °C. The profile looks similar to the blue curve in Figure 7A recorded at 8 °C. From the Guinier analysis we obtain a R_g of 6.5 nm. The scattering curve can be well described by the model of a generalized Gaussian chain with a radius of gyration of 6.7 nm and a ν of 0.40. This nicely agrees with the results from temperature dependent light scattering, where the sample at 25 °C was found to be in the single chain region. Upon increase of the temperature to 65 °C the scattering curve shows an increase of forward scattering. Moreover, a characteristic form factor oscillation becomes visible. We find a similar value of R_g as for the Ca²⁺ sample at 65 °C. From this we conclude that micelles are formed. We employ the same model as used for the Ca²⁺ sample to describe the scattering curve. The resulting aggregation number of 81 is close to the value estimated from static light scattering. In addition, a core radius of 18.3 nm and a value of $R_{g,corona}$ of 1.2 nm is obtained from the analysis. Similarly as for Ca²⁺ the core is highly swollen by water. A micelle containing a PA/Sr²⁺ core is in agreement with the results from ITC since high temperatures promote the entropy driven binding of Sr²⁺ to COO⁻ of the acrylate groups.

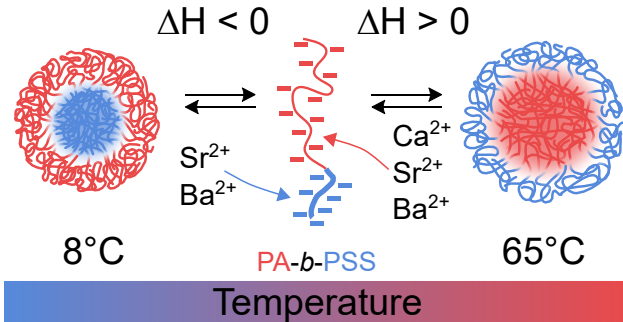
The blue curve in Figure 7B shows the sample at a temperature of 8 °C. Again the forward scattering increases quite dramatically with respect to the single chain state at 25 °C. However, the high q part of the scattering curves is nearly identical with the one of the single chains. This indicates, that the conformation of the PA chains barely changes. Based on this observation and the results obtained from ITC we tried to fit the data with two hypothetical models: one, which assumes that PA complexed by Sr^{2+} forms the core of the micelle and PSS the corona and a second one with PSS/ Sr^{2+} in the core and PA in the corona. The fit was heavily constrained by knowing the molar volumes of the corresponding blocks, scattering length densities and the used polymer concentration. The model assuming a core of PSS/ Sr^{2+} yielded considerably lower values of χ^2 than the one assuming PA/ Sr^{2+} to be in the core. The solid blue line in Figure 7B therefore shows the model based on PSS/ Sr^{2+} cores, whereas Figure S12 in the Supporting Information shows the best fit obtained with PA/ Sr^{2+} in the core. Table 4 summarizes the fitting parameters. The micelles are formed by a rather small core of 7.0 nm formed by PSS/ Sr^{2+} and a considerable amount of water. The PA corona is rather large with $R_{g,\text{corona}}$ of 9.8 nm, which agrees with the fact that the PA block is rather long. The resulting overall dimension of the micelles are in good agreement with the hydrodynamic radius measured by DLS.

Figure 7C shows SANS profiles of the polymer sample in the presence of Ba^{2+} at 8 °C and 65 °C. The sample at the high temperature can be well described by a generalized Gaussian⁴⁷ chain with a radius of gyration of 5.0 nm and ν of 0.26. This is in agreement with the result from DLS and SLS, from which we already expected the polymer to be present as a single chain. In contrast, the curve at 8 °C has a considerably larger forward scattering and shows a well-defined oscillation at $q = 0.19 \text{ nm}^{-1}$. Similarly as for the micelles formed at low temperatures in the presence of Sr^{2+} there are two hypothetical models: PSS/ Ba^{2+} or PA/ Ba^{2+} forming the core of the micelle. Again the model with a core formed by PSS/ Ba^{2+} describes the data considerably better and is shown as a solid blue line in Figure 7C. The alternative model of a PA/ Ba^{2+} core poorly describes the data and is shown in Figure S12.

The obtained micelle dimensions are similar to those of the sample in the presence of Sr^{2+} at low temperatures. The PSS/ Ba^{2+} core is rather small with a radius of 5.6 nm, whereas the PA corona is rather thick with $R_{g,\text{corona}}$ of 8.0 nm.

We were surprised to not observe micelle formation in the presence of Ba^{2+} at high temperatures as the binding of Ba^{2+} to PA is also entropically driven. Therefore, another sample was prepared, this time even closer to the phase boundary. Figure S12 shows the temperature dependent light scattering results of this sample. Similarly as before, micelle formation can be observed at low temperatures but this time also at high temperatures with an intermediate regime of single chains. However, the aggregation numbers and hydrodynamic radius for the micelles at high temperatures are considerably smaller as for Sr^{2+} and Ca^{2+} . We attribute this to the considerably smaller entropy of binding ΔS for the combination PA/ Ba^{2+} , making it harder to trigger the micellization by an increase of the temperature.

We performed similar SANS experiments with the completely hydrogenated polymer $\text{h}_3\text{-PA}_{1190}\text{PSS}_{70}$ in D_2O , which yielded identical temperature behaviors. However, the SANS data on this fully hydrogenated polymer, in particular of the samples with Sr^{2+} and Ba^{2+} at low temperatures, yield similar χ^2 for the model with the PSS/ M^{2+} and the PA/ M^{2+} core. Thus, deuteration of one block is required to be able to differentiate between PA/ M^{2+} and PSS/ M^{2+} in the core of the micelles.



Scheme 1: Illustration of the temperature induced micellization of PA-*b*-PSS in the presence of Ca^{2+} , Sr^{2+} and Ba^{2+} .

To sum up, we found two different temperature dependent trends of PA₁₁₉₀PSS₇₀ in the presence of earth alkaline cations. For all three cations micelle formation can be triggered by increasing the temperature, arising from the strong endothermic binding to the PA block. Consequently, the micelles contain a core formed by PA/M²⁺ and a corona formed by PSS. In contrast, micelle formation at low temperatures can only be observed for Sr²⁺ and Ba²⁺. This micelle formation at low temperatures arises from the exothermic binding of M²⁺ to PSS and consequently leads to a micelle core formed by PSS/M²⁺ and a corona formed by PA. As a result it is possible to generate an invertible micellar system with Sr²⁺ and Ba²⁺, which allows to change the core forming block by a change in temperature.

Conclusion

Polyelectrolytes exhibit ion specific interactions with a large variety of metal cations. This ion specificity depends on the nature of the polyelectrolytes. Ca^{2+} , Sr^{2+} and Ba^{2+} as a representative set of bivalent alkaline earth cations interact specifically with the negative residues of sodium polyacrylates (PA).²⁵⁻²⁷ The interaction is endothermic in nature due to the liberation of water molecules from solvation shells of the ionic residues.^{28,29} Accordingly, addition of those cations to solutions of PA triggers separation of a polymer phase once a threshold of cation concentration is surpassed. An increase of temperature further promotes this phase separation. Unlike to PA, sodium polystyrenesulfonate (PSS) only interacts specifically with Sr^{2+} and Ba^{2+} and the interaction is exothermic in nature.²⁹⁻³¹ Now, the addition of Sr^{2+} and Ba^{2+} triggers phase separation which is further promoted by a decrease in temperature.

The present work makes use of these characteristic and differing interaction patterns in order to present a new route to micelle formation and its inversion by changing the temperature. The new route has been accomplished by combining the different patterns in a PA-*b*-PSS block copolyelectrolyte. As it turned out, the phase separation characteristic to the homo-polyelectrolyte is confined to the respective micellar cores. The starting point is always a solution of the block copolyelectrolytes in their single coil state at a distinct concentration of alkaline earth cations low enough to not yet reach the threshold concentration but large enough to enable induction of micelle formation by a suitable change in temperature.

In the presence of Ca^{2+} micelles are only formed via a temperature increase as this induces neutralization of the PA blocks by the specific bonding of Ca^{2+} to the COO^- residues.²⁰ The PA blocks form the core of the micelles, surrounded by stabilizing PSS blocks. With Sr^{2+} and Ba^{2+} the same types of micelles are generated by an increase of temperature. These micelles are also re-dissolved by decreasing the temperature whereby the state of single coils is reached again. However, a further decrease in temperature generates a new type of micelles, now with PSS blocks in the core being neutralized by either Sr^{2+}

or Ba^{2+} cations respectively and solubilized by dangling PA blocks. This establishes a complete inversion of micelles by a variation of temperature (Scheme 1). The process of micellar inversion could be unambiguously resolved by a combination of SANS with ITC. The morphological changes could be made visible by SANS on a polymer sample with one block of the copolyelectrolyte being fully deuterated. ITC reflected the heat changes accompanying the process of micellar inversion with micelle formation with PA/M^{2+} cores unambiguously related to an endothermic metal cation binding process and micelle formation with PSS/M^{2+} cores at low temperatures to an exothermic metal binding process.

Acknowledgement

This work used the platforms of the Grenoble Instruct center (ISBG; UMS 3518 CNRS-CEA-UJF-EMBL) with support from FRISBI (ANR-10-INSB-05-02) and GRAL (ANR-10-LABX-49-01) within the Grenoble Partnership for Structural Biology (PSB). The authors thank the Institut Laue-Langevin (<https://doi.ill.fr/10.5291/ILL-DATA.9-11-1910>) and the European Synchrotron Radiation Facility for the provision of beam time. The authors gratefully acknowledge the financial support provided by JCNS to perform the neutron scattering measurements at the KWS2 instrument of the Heinz Maier-Leibnitz Zentrum (MLZ), Garching, Germany. The authors thank Aurel Radulescu for fruitful discussions, Caroline Mas for support with the ITC experiments and the Partnership for Soft Condensed Matter (PSCM) for supply of the light scattering. N.C. acknowledges funding for a PhD scholarship from Institut Laue-Langevin.

Supporting Information Available

Additional data including an extensive overview of the fitting parameters with error bars, scattering length densities, measurements of the molar volume of PA and PSS, details regarding the ITC data analysis and description of the synthesis and characterization of all used polymers can be found in the Supporting Information.

References

- (1) Zhang, L.; Eisenberg, A. Multiple Morphologies of "Crew-Cut" Aggregates of Polystyrene-*b*-poly(acrylic acid) Block Copolymers. *Science* (80-.). **1995**, *268*, 1728–1731, DOI: 10.1126/science.268.5218.1728.
- (2) Massey, J.; Nicole Power, K.; Manners, I.; Winnik, M. A. Self-assembly of a novel organometallic-inorganic block copolymer in solution and the solid state: Nonintrusive

- observation of novel wormlike poly(ferrocenyldimethylsilane)-b-Poly (dimethylsiloxane) micelles. *J. Am. Chem. Soc.* **1998**, *120*, 9533–9540, DOI: 10.1021/ja981803d.
- (3) Du, J. Polymer Vesicles. *Adv. Hierarchical Nanostructured Mater.* **2014**, *9783527333*, 177–192, DOI: 10.1002/9783527664948.ch5.
- (4) Schilli, C. M.; Zhang, M.; Rizzardo, E.; Thang, S. H.; Chong, . Y. K.; Edwards, K.; Karlsson, G.; Müller, A. H. E. A New Double-Responsive Block Copolymer Synthesized via RAFT Polymerization: Poly(N -isopropylacrylamide)- b lock -poly(acrylic acid). *Macromolecules* **2004**, *37*, 7861–7866, DOI: 10.1021/ma035838w.
- (5) Lee, A. S.; Gast, A. P.; Bütün, V.; Armes, S. P. Characterizing the structure of pH dependent polyelectrolyte block copolymer micelles. *Macromolecules* **1999**, *32*, 4302–4310, DOI: 10.1021/ma981865o.
- (6) Zhou, S.; Chu, B. Laser light scattering study of pressure-induced micellization of a diblock copolymer of poly(1,1-dihydroperfluorooctylacrylate) and poly(vinyl acetate) in supercritical carbon dioxide. *Macromolecules* **1998**, *31*, 5300–5308, DOI: 10.1021/ma980262+.
- (7) Zhao, Y. Light-responsive block copolymer micelles. *Macromolecules* **2012**, *45*, 3647–3657, DOI: 10.1021/ma300094t.
- (8) Ranka, M.; Katepalli, H.; Blankschtein, D.; Hatton, T. A. Schizophrenic Diblock Copolymer-Functionalized Nanoparticles as Temperature-Responsive Pickering Emulsifiers. *Langmuir* **2017**, *33*, 13326–13331, DOI: 10.1021/acs.langmuir.7b03008.
- (9) Dompé, M.; Cedano-Serrano, F. J.; Heckert, O.; van den Heuvel, N.; van der Gucht, J.; Tran, Y.; Hourdet, D.; Creton, C.; Kamperman, M. Thermoresponsive Complex Coacervate-Based Underwater Adhesive. *Adv. Mater.* **2019**, *31*, DOI: 10.1002/adma.201808179.

- (10) Kotsuchibashi, Y.; Ebara, M.; Aoyagi, T.; Narain, R. Recent advances in dual temperature responsive block copolymers and their potential as biomedical applications. *Polymers (Basel)*. **2016**, *8*, DOI: 10.3390/polym8110380.
- (11) Papadakis, C. M.; Müller-Buschbaum, P.; Laschewsky, A. Switch It Inside-Out: “Schizophrenic” Behavior of All Thermoresponsive UCST–LCST Diblock Copolymers. *Langmuir* **2019**, acs.langmuir.9b01444, DOI: 10.1021/acs.langmuir.9b01444.
- (12) Bütün, V.; Liu, S.; Weaver, J. V. M.; Bories-Azeau, X.; Cai, Y.; Armes, S. P. A brief review of ‘schizophrenic’ block copolymers. *React. Funct. Polym.* **2006**, *66*, 157–165, DOI: 10.1016/j.reactfunctpolym.2005.07.021.
- (13) Feng, A.; Zhan, C.; Yan, Q.; Liu, B.; Yuan, J. A CO₂- and temperature-switchable “schizophrenic” block copolymer: from vesicles to micelles. *Chem. Commun. (Cambridge, U. K.)* **2014**, *50*, 8958–8961, DOI: 10.1039/C4CC03156C.
- (14) Wang, D.; Wu, T.; Wan, X.; Wang, X.; Liu, S. Purely salt-responsive micelle formation and inversion based on a novel schizophrenic sulfobetaine block copolymer: Structure and kinetics of micellization. *Langmuir* **2007**, *23*, 11866–11874, DOI: 10.1021/1a702029a.
- (15) Vasantha, V. A.; Jana, S.; Lee, S. S.-C.; Lim, C.-S.; Teo, S. L.-M.; Parthiban, A.; Vancso, J. G. Dual hydrophilic and salt responsive schizophrenic block copolymers – synthesis and study of self-assembly behavior. *Polym. Chem.* **2015**, *6*, 599–606, DOI: 10.1039/C4PY01113A.
- (16) Guragain, S.; Bastakoti, B. P.; Nakashima, K. Schizophrenic micellization of poly(ethylene oxide-*b*-methacrylic acid) induced by phosphate and calcium ions. *J. Colloid Interface Sci.* **2010**, *350*, 63–68, DOI: 10.1016/j.jcis.2010.06.007.
- (17) Vishnevetskaya, N. S.; Hildebrand, V.; Niebuur, B.-J.; Grillo, I.; Filippov, S. K.; Laschewsky, A.; Müller-Buschbaum, P.; Papadakis, C. M.

- “Schizophrenic” Micelles from Doubly Thermoresponsive Polysulfobetaine- b -poly(N -isopropylmethacrylamide) Diblock Copolymers. *Macromolecules* **2017**, *50*, 3985–3999, DOI: 10.1021/acs.macromol.7b00356.
- (18) Vishnevetskaya, N. S.; Hildebrand, V.; Dyakonova, M. A.; Niebuur, B. J.; Kyriakos, K.; Raftopoulos, K. N.; Di, Z.; Müller-Buschbaum, P.; Laschewsky, A.; Papadakis, C. M. Dual Orthogonal Switching of the ”schizophrenic” Self-Assembly of Diblock Copolymers. *Macromolecules* **2018**, *51*, 2604–2614, DOI: 10.1021/acs.macromol.8b00096.
- (19) Liu, S.; Billingham, N. C.; Armes, S. P. A schizophrenic water-soluble diblock copolymer. *Angew. Chemie - Int. Ed.* **2001**, *40*, 2328–2331, DOI: 10.1002/1521-3773(20010618)40:12<2328::AID-ANIE2328>3.0.CO;2-M.
- (20) Carl, N.; Prévost, S.; Schweins, R.; Huber, K. Ion-selective binding as a new trigger for micellization of block copolyelectrolytes with two anionic blocks. *Soft Matter* **2019**, DOI: 10.1039/C9SM01138B.
- (21) Yap, H. P.; Hao, X.; Tjipto, E.; Gudipati, C.; Quinn, J. F.; Davis, T. P.; Barner-Kowollik, C.; Stenzel, M. H.; Caruso, F. Synthesis, multilayer film assembly, and capsule formation of macromolecularly engineered acrylic acid and styrene sulfonate block copolymers. *Langmuir* **2008**, *24*, 8981–8990, DOI: 10.1021/1a8011074.
- (22) Förster, S.; Hermsdorf, N.; Böttcher, C.; Lindner, P. Structure of polyelectrolyte block copolymer micelles. *Macromolecules* **2002**, *35*, 4096–4105, DOI: 10.1021/ma011565y.
- (23) van der Maarel, J. R. C.; Groenewegen, W.; Egelhaaf, S. U.; Lapp, A. Salt-Induced Contraction of Polyelectrolyte Diblock Copolymer Micelles. *Langmuir* **2000**, *16*, 7510–7519, DOI: 10.1021/1a000299z.
- (24) Hansch, M.; Hämisch, B.; Schweins, R.; Prévost, S.; Huber, K. Liquid-liquid phase separation in dilute solutions of poly(styrene sulfonate) with multivalent cations: Phase

- diagrams, chain morphology, and impact of temperature. *J. Chem. Phys.* **2018**, *148*, 014901, DOI: 10.1063/1.5006618.
- (25) Schweins, R.; Goerigk, G.; Huber, K. Shrinking of anionic polyacrylate coils induced by Ca²⁺, Sr²⁺ and Ba²⁺: A combined light scattering and ASAXS study. *Eur. Phys. J. E* **2006**, *21*, 99–110, DOI: 10.1140/epje/i2006-10047-7.
- (26) Lages, S.; Schweins, R.; Huber, K. Temperature-Induced Collapse of Alkaline Earth Cation-Polyacrylate Anion Complexes. *J. Phys. Chem. B* **2007**, *111*, 10431–10437, DOI: 10.1021/jp068258k.
- (27) Huber, K. Calcium-induced shrinking of polyacrylate chains in aqueous solution. *J. Phys. Chem.* **1993**, *97*, 9825–9830, DOI: 10.1021/j100140a046.
- (28) Sinn, C. G.; Dimova, R.; Antonietti, M. Isothermal Titration Calorimetry of the Polyelectrolyte/Water Interaction and Binding of Ca²⁺ : Effects Determining the Quality of Polymeric Scale Inhibitors. *Macromolecules* **2004**, *37*, 3444–3450, DOI: 10.1021/ma030550s.
- (29) Hansch, M.; Kaub, H. P.; Deck, S.; Carl, N.; Huber, K. Reaction enthalpy from the binding of multivalent cations to anionic polyelectrolytes in dilute solutions. *J. Chem. Phys.* **2018**, *148*, 114906, DOI: 10.1063/1.5019877.
- (30) Prabhu, V.; Muthukumar, M.; Wignall, G.; Melnichenko, Y. Dimensions of polyelectrolyte chains and concentration fluctuations in semidilute solutions of sodium–poly(styrene sulfonate) as measured by small-angle neutron scattering. *Polymer (Guildf)*. **2001**, *42*, 8935–8946, DOI: 10.1016/S0032-3861(01)00382-2.
- (31) Prabhu, V. M.; Muthukumar, M.; Wignall, G. D.; Melnichenko, Y. B. Polyelectrolyte chain dimensions and concentration fluctuations near phase boundaries. *J. Chem. Phys.* **2003**, *119*, 4085–4098, DOI: 10.1063/1.1592496.

- (32) Lee, C. L.; Muthukumar, M. Phase behavior of polyelectrolyte solutions with salt. *J. Chem. Phys.* **2009**, *130*, 1–9, DOI: 10.1063/1.3054140.
- (33) Kanai, S.; Muthukumar, M. Phase separation kinetics of polyelectrolyte solutions. *J. Chem. Phys.* **2007**, *127*, 244908, DOI: 10.1063/1.2806299.
- (34) Zemb, T.; Lindner, P. *Neutrons, X-rays and light: scattering methods applied to soft condensed matter*; North-Holland, 2002.
- (35) Zentrum, H. M.-L. KWS-2 : Small angle scattering diffractometer. *J. large-scale Res. Facil.* **2015**, *A29*, 2–6, DOI: <http://dx.doi.org/10.17815/jlsrf-1-27>.
- (36) Houston, J. E.; Brandl, G.; Drochner, M.; Kemmerling, G.; Engels, R.; Papagiannopoulos, A.; Sarter, M.; Stadler, A.; Radulescu, A. The high-intensity option of the SANS diffractometer KWS-2 at JCNS – characterization and performance of the new multi-megahertz detection system. *J. Appl. Crystallogr.* **2018**, *51*, 323–336, DOI: 10.1107/S1600576718004132.
- (37) Orthaber, D.; Bergmann, A.; Glatter, O. SAXS experiments on absolute scale with Kratky systems using water as a secondary standard. *J. Appl. Crystallogr.* **2000**, *33*, 218–225, DOI: 10.1107/S0021889899015216.
- (38) Boesecke, P. Reduction of two-dimensional small- and wide-angle X-ray scattering data. *J. Appl. Crystallogr.* **2007**, *40*, 423–427, DOI: 10.1107/S0021889807001100.
- (39) Frisken, B. J. Revisiting the method of cumulants for the analysis of dynamic light-scattering data. *Appl. Opt.* **2001**, *40*, 4087, DOI: 10.1364/AO.40.004087.
- (40) Burchard, W.; Schmidt, M.; Stockmayer, W. H. Influence of Hydrodynamic Preaveraging on Quasi-Elastic Scattering from Flexible Linear and Star-Branched Macromolecules. *Macromolecules* **1980**, *13*, 580–587, DOI: 10.1021/ma60075a020.

- (41) Burchard, W.; Schmidt, M.; Stockmayer, W. H. Information on Polydispersity and Branching from Combined Quasi-Elastic and Intergrated Scattering. *Macromolecules* **1980**, *13*, 1265–1272, DOI: 10.1021/ma60077a045.
- (42) Cho, C. H.; Urquidi, J.; Singh, S.; Robinson, G. W. Thermal Offset Viscosities of Liquid H₂O, D₂O, and T₂O. *J. Phys. Chem. B* **1999**, *103*, 1991–1994, DOI: 10.1021/jp9842953.
- (43) Zimm, B. H. The Scattering of Light and the Radial Distribution Function of High Polymer Solutions. *J. Chem. Phys.* **1948**, *16*, 1093–1099, DOI: 10.1063/1.1746738.
- (44) Muthig, M.; Prévost, S.; Orglmeister, R.; Gradzielski, M. SASET: A program for series analysis of small-angle scattering data. *J. Appl. Crystallogr.* **2013**, *46*, 1187–1195, DOI: 10.1107/S0021889813016658.
- (45) Pedersen, J. S.; Posselt, D.; Mortensen, K. Analytical treatment of the resolution function for small-angle scattering. *J. Appl. Crystallogr.* **1990**, *23*, 321–333, DOI: 10.1107/S0021889890003946.
- (46) Debye, P. Molecular-weight determination by light scattering. *J. Phys. Colloid Chem.* **1947**, *51*, 18–32, DOI: 10.1021/j150451a002.
- (47) Hammouda, B. SANS from homogeneous polymer mixtures: A unified overview. *Polym. Charact.* **1993**, *106*, 87–133, DOI: 10.1007/BFb0025862.
- (48) Pedersen, J. S.; Gerstenberg, M. C. Scattering Form Factor of Block Copolymer Micelles. *Macromolecules* **1996**, *29*, 1363–1365, DOI: 10.1021/ma9512115.
- (49) Pedersen, J. S.; Svaneborg, C. Scattering from block copolymer micelles. *Curr. Opin. Colloid Interface Sci.* **2002**, *7*, 158–166, DOI: 10.1016/S1359-0294(02)00044-4.
- (50) Svaneborg, C.; Pedersen, J. S. Form Factors of Block Copolymer Micelles with

- Excluded-Volume Interactions of the Corona Chains Determined by Monte Carlo Simulations. *Macromolecules* **2002**, *35*, 1028–1037, DOI: 10.1021/ma011046v.
- (51) Pedersen, J. S.; Svaneborg, C.; Almdal, K.; Hamley, I. W.; Young, R. N. A Small-Angle Neutron and X-ray Contrast Variation Scattering Study of the Structure of Block Copolymer Micelles: Corona Shape and Excluded Volume Interactions. *Macromolecules* **2003**, *36*, 416–433, DOI: 10.1021/ma0204913.
- (52) Rayleigh, L. Form factor of a homogenous sphere. *Proc. Roy. Soc. London* **1911**, *A84*, 25–38.
- (53) Svaneborg, C.; Pedersen, J. S. Block copolymer micelle coronas as quasi-two-dimensional dilute or semidilute polymer solutions. *Phys. Rev. E* **2001**, *64*, 010802, DOI: 10.1103/PhysRevE.64.010802.
- (54) Skov, J.; Schurtenberger, P.; Pedersen, J. S. Scattering Functions of Semiflexible Polymers with and without Excluded Volume Effects Excluded Volume Effects. *Macromolecules* **1996**, *9297*, 7602–7612, DOI: 10.1021/ma9607630.
- (55) Chen, W. R.; Butler, P. D.; Magid, L. J. Incorporating intermicellar interactions in the fitting of SANS data from cationic wormlike micelles. *Langmuir* **2006**, *22*, 6539–6548, DOI: 10.1021/1a0530440.
- (56) Sommer, C.; Pedersen, J. S.; Garamus, V. M. Structure and interactions of block copolymer micelles of brij 700 studied by combining small-angle X-ray and neutron scattering. *Langmuir* **2005**, *21*, 2137–2149, DOI: 10.1021/1a047489k.
- (57) Mizoue, L. S.; Tellinghuisen, J. The role of backlash in the "first injection anomaly" in isothermal titration calorimetry. *Anal. Biochem.* **2004**, *326*, 125–127, DOI: 10.1016/j.ab.2003.10.048.

- (58) Turnbull, W. B.; Daranas, A. H. On the Value of c : Can Low Affinity Systems Be Studied by Isothermal Titration Calorimetry? *J. Am. Chem. Soc.* **2003**, *125*, 14859–14866, DOI: 10.1021/ja036166s.
- (59) Scheuermann, T. H.; Brautigam, C. A. High-precision, automated integration of multiple isothermal titration calorimetric thermograms: New features of NITPIC. *Methods* **2015**, *76*, 87–98, DOI: 10.1016/j.ymeth.2014.11.024.
- (60) Stuhrmann, H. B. Neutron small-angle scattering of biological macromolecules in solution. *J. Appl. Crystallogr.* **1974**, *7*, 173–178, DOI: 10.1107/S0021889874009071.
- (61) Schweins, R.; Huber, K. Collapse of sodium polyacrylate chains in calcium salt solutions. *Eur. Phys. J. E* **2001**, *5*, 117–126, DOI: 10.1007/s101890170093.
- (62) Huber, K. Calcium-induced shrinking of polyacrylate chains in aqueous solution. *J. Phys. Chem.* **1993**, *97*, 9825–9830, DOI: 10.1021/j100140a046.
- (63) Matulis, D.; Rouzina, I.; Bloomfield, V. A. Thermodynamics of DNA binding and condensation: isothermal titration calorimetry and electrostatic mechanism. *J. Mol. Biol.* **2000**, *296*, 1053–1063, DOI: 10.1006/jmbi.1999.3470.

Graphical TOC Entry

